The effect of centre bow and wet-deck geometry on wet-deck slamming loads and vertical bending moments of wave-piercing catamarans

Babak Shabani [a,*], Jason Lavroff [a], Damien S Holloway [a], Michael R Davis [a] and Giles A Thomas [b]

[a] School of Engineering and ICT, University of Tasmania, Private Bag 65, Hobart 7000, Australia

[b] Department of Mechanical Engineering, University College London, England, United Kingdom

* Corresponding author. Email address: babak.shabani@utas.edu.au

Abstract

An experimental study was performed to determine the influence of centre bow length and tunnel height on the magnitude of the wave slamming loads and bending moments acting on a 112 m Incat wave-piercer catamaran vessel. A 2.5 m hydroelastic segmented catamaran model was tested in regular head sea waves at a high model speed in multiple test series, whilst five centre bow (CB) and wet-deck configurations were considered, designated here as the parent, low, high, long and short CBs. The model global motions, centre bow slam loads, accelerations, and slam induced vertical bending moments of the catamaran model in waves were measured. It was found that the slam force, the centre bow entry force and slam induced bending moment all increase as the centre bow length increases. Increasing the wet-deck height increased the motions but reduced the maximum slam load in moderate waves. It was seen that the short CB was the best design for the alleviation of slam load. The high CB was the second best choice for operation in moderate waves but it was the worst configuration in terms of heave and pitch motions among various CB configurations tested.

Key words: Catamaran; Hydroelastic segmented model; Wet-deck slamming; Center bow; Relative motions; Vertical bending moment

1 Introduction

Large wave-piercing catamarans (WPCs) are an economic option for fast sea transportation. Since the 1990s many large WPCs have been constructed at the Incat Tasmania Hobart shipyard, ranging from 74 m to 112 m in overall length and operated mainly as passenger/vehicle ferries. These aluminium vessels have a distinctive design with an above water centre bow connecting two

demihulls in the forward region as shown in Figure 1(a). The centre bow in wave-piercing catamarans provides reserve buoyancy for minimising deck diving in following seas.

In WPCs with a centre bow, wet-deck slamming is one of the main sources of loading to be considered in structural design (Thomas et al., 2003b). The structural design process is complicated as the centre bow immersion in waves can lead to arch filling and slamming (Davis et al., 2009; Lavroff et al., 2013b). When the bow is deeply submerged, the water fills the archways, and consequently large transient slam loads may occur, generating whipping and structural vibrations (Lavroff et al., 2009; Thomas et al., 2003a; Thomas et al., 2011). In the long term, these vibrations need to be evaluated for possible fatigue damage (Thomas et al., 2006). The wet-deck slamming in the archway area can also generate extreme quasi-static loads with the potential to damage the vessel structure (Amin, 2009).

The severity of slam forces on WPCs with a centre bow can be significant. Amin (2009) used strain data from a 98 m Incat vessel obtained during sea trials and compared these with dynamic finite element analyses to identify the corresponding slam loads. A maximum slam force of 2274 tonnes at a speed of 20 knots in sea state 5 was identified for the 98 m vessel during the sea trails. An extreme asymmetric slam force acting on only one side of the centre bow of the 96 m vessel was estimated to be 1025 tonnes (Thomas, 2003). On the basis of model tests in random wave head seas Davis et al. (2017) reported a maximum slam force (full-scale equivalent) of over 34300 kN at a speed of 38 knots in 3.5 m significant wave height seas, noting that the model was tested at a displacement that was approximately 10% greater than the design displacement.

Thomas (2003) showed the slam occurrence rate for an 86 m WPC was significant even in speeds between 10 and 15 knots in significant wave heights of 2.5 to 3 m; it should be noted that the operational wet deck (or tunnel) clearance of the vessel in the study was 2.34 m. Slamming events were also identified in smaller waves in the range of 1.5 to 2 m. However, the study indicated that the vast majority of slam events were relatively small in magnitude and the small slams were more important for their effect on fatigue life than for ultimate strength considerations.

Passenger/vehicle ferries that are repeatedly exposed to slamming are required to reduce speed or change course to avoid both structural damage and passenger discomfort. These operational manoeuvres reduce the ship transport efficiency. There is also a class service regulation for reduction of the speed depending on the significant wave height (Faltinsen, 2005) for ferry operations. For vessels that are often exposed to minor slamming, the speed reduction based on the rate of slamming is not practically significant as these many small slamming loads do not have a significant effect on structural reliability. Ideally, only moderate or severe slamming loads need to be avoided. The severity of slamming, as

mentioned earlier, can be in excess of the vessel weight with some potential damage to the hull's structure such as buckling of the hull near the bridge as shown in Figure 1(b). Thus, a suitable approach would be to follow a speed reduction criterion based on both occurrence rate and severity of slamming loads so as to maintain high speed in low risk environments and to avoid encountering severe and detrimental slamming events. At sea, however, there would be no choice but to minimise slamming severity and occurrences through speed reduction as the environmental conditions are beyond control. In the design stage it is possible to minimise the slamming effect on the ship structure and increase the transport efficiency by hull design modifications such as those considered in this paper or by implementing other motion reduction techniques such as ride control systems (AlaviMehr et al., 2017a).

Two design parameters that could potentially have a significant effect on slamming behaviour of WPCs are the centre bow length and wet deck height, although it must be borne in mind that these two parameters also affect the reserve buoyancy provided by the centre bow. Since slamming is a consequence of high relative vertical motion (Dessi and Ciappi, 2013; Ochi, 1964; Ochi and Motter, 1973), the rate of slamming occurrence could be decreased by increasing the tunnel clearance provided that the vertical motions do not also increase with this increase. The overall objective of this paper is to investigate the effects of the centre bow length and wet-deck height (i.e. the tunnel clearance) on the slam loads of wave-piercing catamarans as investigations in the most recent research undertaken to date have not considered the effect on slam loadings of variation of these parameters for the bow geometry of WPCs (Rafie Shahraki, 2014).

Application of established and well-known analytical methods such as those in (Faltinsen and Chezhian, 2005; Von Karman, 1929; Wagner, 1932; Zhao and Faltinsen, 1993) is not straightforward for slam load identification of WPCs with a centre bow. Two main limitations can be identified in using analytical approaches for direct slam impact load and indirect slam-induced load estimations. Firstly, there is an overestimation of slam loads by using simplified two dimensional numerical methods. Davis et al. (2010) have shown this overestimation for Incat vessel sections to be as much as a factor of three. Secondly, Wagner-type theories are based on a rigid body hydrodynamic approach. This means that in the Wagner-type methods dynamic structural considerations including hydroelasticity effects are not combined with the hydrodynamic theories. Integrating structure and hydrodynamic effects is a critical design necessity for WPCs as for this class of vessel the time scale of slam events is comparable with the whipping vibratory period of the hull (Thomas et al., 2003b & 2006). Consequently structure-fluid interaction effects influence the full vessel response and it is not sufficient to merely predict the local slam force magnitude on the basis of hydrodynamics alone. Thus we require both model testing and computational analyses to model the hydro-elastic response in order to determine the slamming severity and occurrence rate. Model test data can

then be applied to the development of algorithms for the prediction of motions, slam loads and structural dynamic response.

The use of Computational Fluid Dynamics (CFD) for slam load identification in Incat vessels is at an early stage for practical or routine use (McVicar et al., 2016). McVicar et al. (2014) presented a method for estimation of transient slam force of a hydroelastic segmented model (HSM) based on the global motions and hull bending responses. The method was based on RANSE simulation and dynamic modelling of a 2.5 m hydroelastic segmented model based on the 112 m Incat WPC. The CFD simulations for the centre bow design can be computationally expensive and excessively time consuming for a ship design office and also require experimental data for validation (Lavroff et al., 2011).

Full-scale trials still remain an effective method of research for ship slamming (Kapsenberg, 2011). Thomas et al. (2003b) conducted full-scale measurements on two Incat vessels with 86 and 96 m overall length. The majority of slams were found to be less than 20% of the most severe slam load observed in full-scale trials. This indicated the importance of structural design to protect against slam-induced fatigue (Thomas et al., 2003c; Thomas et al., 2004, 2005, 2008): this has not been comprehensively formulated by classification societies to date. It was also found by Thomas et al. that the extreme slam load resulted in a greater slam induced bending moment than that obtained by application of the DNV rules (Thomas et al., 2002), noting that the effect of the centre bow on the design hogging and sagging bending moment has not so far been accommodated in the rules.

Generally however, it is not possible to determine the most likely severe slam loads over the lifetime of the vessel on the basis of full-scale measurements for a prescribed set of conditions because slamming is usually avoided during ship operations by either course changes or speed reductions so as to minimise damage sustained by the vessel. In addition, the extreme slam loads can be greatly influenced by the centre bow configuration (Rafie Shahraki, 2014), but the results from the full-scale investigations have yet to be used directly for slam load estimates for different designs due to the complexity arising from the random nature of encountered waves. The model test technique thus provides the best opportunity to study severe slamming conditions in a controlled test environment, allowing variation of test conditions and parameters to identify peak slam conditions. A variety of hull configurations can also be easily tested with an extensive set of instruments, and a direct design approach can then be formulated to account for centre bow effects on both motions and slam loads.

Hydroelastic models are thus seen to be appropriate for slamming research. Dessi (2013) and Dessi and Mariani (2008) used a segmented hydroelastic model for reconstruction of slam-induced loads and bottom slamming loads of a high-speed monohull. Ge et al. (2002) also used a three segmented catamaran model to

study wet-deck slamming on a catamaran. Two similar sized hydroelastic segmented models (HSM01 and HSM02) based on 112 m Incat WPC have been designed, built and used since 2007 at the University of Tasmania (French, 2012; Lavroff, 2009; Matsubara, 2009; Rafie Shahraki, 2014). Initially, Matsubara (2009) and Lavroff (2009) developed HSM01 to investigate slam loads, whipping vibrations and global motions of the model catamaran in regular waves. The effect of speed and wave height on motions and slamming of the catamaran model was found to be significant in regular waves (Lavroff et al., 2013a). French (2012) also conducted testing using HSM01 in irregular waves and French et al. (2013 & 2014) studied the occurrences and characteristics of slamming events in irregular waves. In a more recent study, the HSM01 model was fitted with a ride control system (RCS) to investigate the effect of the RCS on motions and loads of the catamaran model (AlaviMehr, 2016; AlaviMehr et al., 2017a, b). The study demonstrated the effectiveness of a ride control system (comprising T foil and stern tabs) for mitigation of wave slamming loads by reducing motions.

The centre bow mounting arrangement of HSM01 was redesigned in the second hydroelastic segmented model, HSM02, to allow substitution of different centre bows and variation of the tunnel clearance and height of the flat main wet deck. The work presented here used HSM02 to investigate variations of the wet deck height and centre bow length to investigate the influence of these parameters on the wave induced slam loads and bending moment response.

2 Test facilities and model set-up

2.1 Towing tank and catamaran model

Model tests were performed at the Australian Maritime College (AMC), which is 100 m long and 3.55 m wide and was filled to 1.4 m depth. The tank is equipped with a paddle type wavemaker, a stationary wave probe, side beaches, towing carriage and a sloping beach at the end. The 2.5 m catamaran model HSM02 representing the 112 m Incat WPC was used for tank testing. The model was developed specifically for the AMC towing tank by considering the effective length of the tank and a maximum Froude number of 0.62 for the model. The model was segmented and hydroelastic links were used to connect the demihulls segments to replicate a whipping frequency of 13.79 Hz, representing a whipping frequency of 2.06 Hz at full-scale (Lavroff et al., 2009).

As shown in Figure 2(a), the model comprised four main segments (centre bow, forward demihulls, midship section and aft section) with two cuts placed longitudinally at 33% and 56% of the model overall length from the transom. Since one of the main objectives of the model design was to measure slamming loads acting on the arched wet-deck cross structure between the centre bow and demihulls, in the forward segment the centre bow and the wet-deck were constructed as one part, referred to here as the centre bow (CB) segment, which was suspended between the forward port and starboard demihull segments.

Figure 2(b) shows exploded views of the demihulls and flat wet-deck of the catamaran model and the centre bow. When assembled the sides of the CB segment were separated from the demihulls by about 10 mm gaps, and the CB itself was mounted on two transverse aluminium beams (T-beams) with two load cells located below the transverse beams on the centre line of the model. The centre bow segment was changeable and could be replaced by alternate designs that had different wet-deck heights. Therefore, the flat deck plates in the middle and aft segments were designed to be vertically adjustable to allow necessary alignment according to the wet-deck installed on the forward segment.

Four links were used to connect the forward, middle and aft model segments. Each link had an overall length of 100 mm and the smaller cross section in the middle of the link was designed to produce the required rigidity in bending at model scale to replicate the first two full scale longitudinal modal frequencies (Lavroff et al., 2009). The two ends of each link were fitted and bolted inside the hollow section of square backbone aluminium beams built into the demihulls. Figure 3 shows schematic views of the catamaran model illustrating the configuration of the backbone aluminium beams and the locations of the elastic links at forward and aft cuts on port and starboard sides.

The principal particulars of the 2.5 m model constructed from carbon fibre and Divinycell foam sandwich and the full-scale catamaran are given in Table 1. The model had a lightweight structure of about 20 kg but a displacement of 27.12 kg was required to represent a full-scale 2500 tonnes. The details of the mass distribution in the 2.5 m catamaran model are presented in Table 2. The pitch radii of gyration for the model and the segments were measured using the bifilar suspension method (Lavroff, 2009), the overall radius of gyration in the model being correctly scaled from full scale at 27.5% of the overall length.

Table 1 Principal particulars of the HSM02 model and the 112 m Incat catamaran

	Catamaran Model (HSM02)	Full scale 112m Incat Catamaran
Overall length	2.5 m	112.6 m
Length (waterline)	2.36 m	105.6 m
Displacement	27.12 kg	2500 tonnes
Overall beam	0.68 m	30.5 m
Beam of demihulls	0.13 m	5.8 m
LCG (from transom)	0.941 m	42.15 m
Pitch radius of gyration (about LCG)	0.69 m	30.91 m

Table 2 Details of the catamaran model segments

	Length (% overall length)	Mass (% total mass)	Pitch radius of gyration (m)
Forward segment	44	31	0.22
Middle segment	23	29	0.18
Aft segment	33	40	0.17

2.2 Variable bow configurations

Five centre bow (CB) configurations, designated the parent, high, low, long and short CBs, were considered to investigate the effect of the tunnel clearance and centre bow length on motions and loads of wave-piercing catamarans. The parent CB represents the centre bow of the 112 m Incat catamaran at model scale, as shown in Figure 4. The low CB and high CB, have lower and higher wet-deck clearances respectively (i.e. tunnel clearances) compared with the parent centre bow, and the long CB and short CB, have longer and shorter overall length when compared to the parent CB.

As shown in Figure 5, the tunnel or wet deck clearance is defined here as the height of the underside of the wet-deck above the design waterline at the midship position, and the centre bow length is defined as the longitudinal distance from the centre bow truncated section to the foremost bow position. Tunnel height is defined as the vertical distance from the model keel line to the wet-deck at the midship section.

Figure 6(a) shows the model with the short CB. The short CB configuration was obtained by removing the aft 25% of the parent CB length from its truncation, and the long CB was made by adding an extender, also 25% of the parent CB length. Figure 6(b) shows photographs of the parent CB and long CB extenders. As can be seen in 6(b) the cross-section area becomes wider with the increase of the centre bow length, noting that the centre bow length ranges between 18% and 30% of the overall length.

Figure 7 shows photographs of the catamaran model with the low and high CBs at the initial stage of towing in calm water. The range of variation of the tunnel clearance is between 2% and 3.8% of the overall length. Table 3 summarises design parameters for various CB configurations for the both model and full-scale vessel.

Table 3 Design parameters for various CB configurations

	Model scale			**Full scale**		
	Tunnel height (mm)	Tunnel clearance (mm)	Centre bow length (mm)	Tunnel height (m)	Tunnel clearance (m)	Centre bow length (m)
High CB	177.8	94.2	608	7.97	4.22	27.24
Parent CB	150.5	66.8	608	6.74	2.99	27.24
Low CB	135.3	51.7	608	6.06	2.32	27.24
Long CB	150.5	66.8	758	6.74	2.99	33.96
Short CB	150.5	66.8	458	6.74	2.99	20.52

2.3 Instrumentation

The model was instrumented with a set of sensors as listed in Table 4. With reference to Table 4, the ATI force/moment sensors were used to measure the centre bow loads. The Brüel & Kjær accelerometers were used to keep records of the centre bow accelerations in waves and slamming. The strain gauges were installed on the elastic links to measure vertical bending moments due to global wave loads and slam-induced loads. Two strain gauges were used for each of the elastic links on top

and bottom surface in a half-bridge configuration to sense vertical bending moment directly in terms of the differential stain between the top and bottom surfaces of each link. The model vertical motions were measured using towing posts located on the mid and aft segments by using two Linear Variable Differential Transducers (LVDTs), with the model being only free to move in pitch and heave. The water level was set to 1.4 m to provide a sufficient clearance to the underneath of the carriage to avoid a collision when the vertical motions at the bow were large**.** The generated waves were measured by a stationary resistive type wave probe located in front of the wavemaker by a distance of 9 m. The static wave measurements were used to obtain the wave height and frequency in each single run. Two other resistive-type wave probes were used as the moving wave probes attached to the carriage to identify the encountered wave phase. The carriage speed was set manually at the required constant speed and its variation recorded during each test run. A LabVIEW program was used to record and monitor signals digitised by an M series National Instrument data acquisition card. Figure 8 shows the locations of the sensors installed on the catamaran model.

Table 4 List of instrument used in HSM02 model test

Sensors	Quantity	Description
Load cell (LC)	2	Mini 45 ATI force/moment transducers
LVDT	2	Linear Variable Differential Transformers
Static wave probe	1	Resistive type
Moving wave probe	2	Resistive type
Strain gauge (SG)	4 pairs	350 Ohm , miniature type
Accelerometer (A)	2	Brüel & Kjær accelerometers
DAQ	1	National Instruments

* Refer to Figure 8 for the positions of the sensors.

2.4 Model test conditions

The models were tested in regular waves in head seas in the two wave height test conditions given in Table 5. Multiple wave frequencies were selected for these two test conditions. Test condition 2 presents an unrealistic condition for full-scale commercial vessel operations as the speed would normally be reduced in 4 m waves based on class speed restrictions. However, it was intentionally

selected outside the normal operating envelope so as to consider the effect of the speed on loads in larger waves which might sometimes occur during military operations.

Table 5 Model test conditions

	Model scale		Full-scale	
	Velocity	Wave height	Velocity	Wave height
	V_m (m/s)	h_w (mm)	V_s (knots)	H (m)
Condition 1	2.89	60	38	2.7
Condition 2	2.89	90	38	4.0

2.5 The centre bow load identification and measurement

Slamming events on the catamaran model were identified by analysing the load and acceleration signals measured on the centre bow segment. Scale model slamming with the parent CB has been extensively investigated in previous studies in both regular and irregular waves (Lavroff (2009), French (2012)). Most of the previous model tests were performed using an earlier model of the 112 m Incat vessel (HSM01). The load measurements performed using the HSM01 catamaran model were conducted with limited direct measurement of the CB segment accelerations during slamming. Therefore, the effect of CB inertial loads on slam load measurement was estimated (Lavroff, 2009) or was considered by an indirect approach such as using the heave and pitch acceleration to estimate inertia of the CB segment (French, 2012). However in the present study the inertia loads were calculated directly using data obtained from Brüel & Kjær accelerometers. It has been shown that the CB acceleration caused by slamming loads is superimposed upon the CB acceleration due to the heave and pitch motions. Further, the inertia loads can be underestimated if the effect of slamming loads on the CB acceleration is ignored.

In order to measure the centre bow hydrodynamic and slam loads, the centre bow was built separately from the forward segments and soft, thin and flexible latex bands with low tension were used to cover and seal the gaps between demi hulls and the centre bow. The effect of these latex seals on the transmission of load between segments was small but was essentially allowed for by direct calibration of the load sensors in the fully assembled model. The two aluminium transverse beams fixed on the forward segment demi hulls were used as supports for the centre bow segment, and at each support point an ATI force/moment sensor was located to measure the transmitted loads and moments caused by wave and slam loads. A square aluminium plate was built on the centre line of the

centre bow segment to provide a flat contact surface for the loading face of each force/moment sensor. The connections of the centre bow segment and transverse beams were fixed using four bolts, one on each corner of each built-in square plate. Figure 9 provides schematic details of the centre bow segment and the location of the force/moment sensors. The CB segment mass was 2.7 kg, with the overall length of 1.1 m, and its centre of gravity was located approximately underneath the forward transverse beam.

Equation 1 describes the dynamic equilibrium of the CB segment at its centre of gravity,

$$\sum F_z = F_z^{\mathrm{CB}} + F_z^{\mathrm{aft}} + F_z^{\mathrm{fwd}} = m_{cb}.a_z \qquad (1)$$

where F_z denotes vertical force acting on the centre bow, F_z^{CB} denotes external hydrodynamic forces, F_z^{aft} denotes aft mounting load, F_z^{fwd} denotes forward mounting load, a_z denotes vertical CB acceleration and m_{cb} denotes the mass of the CB segment.

The acceleration signals measured on the CB segments were filtered using a 5th order low-pass Butterworth filter with a 200 Hz cut-off. Figure 10 shows a comparison of the CB segment acceleration between the measured data and filtered data. The CB segment was accelerated due to the catamaran model motions, the forward segment vibrations (mainly due to whipping), the slamming force and self-vibrations on its mountings. These accelerations had different frequencies, and they were superimposed on the measured acceleration signals as shown in Figure 10. The filtering removed the self-vibrations of the CB on its mountings. A maximum CB vertical acceleration after filtering of $3.5g$ was measured during the experiments and it was found that the slamming significantly contributed to the total vertical acceleration. Since the mass of the CB segment was approximately 10% of the catamaran model displacement, the CB vertical inertia loads were quite significant depending on the CB slam acceleration.

Identification of a slam event was based on impulsive responses measured simultaneously by the centre bow accelerometers, centre bow load cells and the whipping responses recorded by the strain gauges. The slamming instants were considered to be the time of peak CB external force obtained using Equation 1. Figure 11 shows the summation of loads measured at the mounts by the forward and aft load cells (top) and the inertia force (middle) identified for a sample run at a speed of 2.89 m/s in 90 mm waves. The lower graph in this figure shows the difference, F_z^{CB}, which is the external hydrodynamic CB force. It can be seen that the whipping frequency affected both the CB load and

inertia recorded. While the centre bow was out of the water, the whipping caused vibrations in the inertia loads that were approximately equal but opposite to that measured by the load cells at the whipping frequency. As a result, the whipping did not create a significant external force prior to slamming or during the centre bow entry. However immediately after each slam, when the centre bow was still in the water, the added mass effect likely provided extra imbalances and m_{CB} in Equation 1 was no longer the mass of the CB segment. It should be noted that the added mass was not measured but the added mass effect on the load CB external force signal can be seen through the decaying vibrations occurring at the whipping frequency after the peak slamming load as shown in Figure 11. See also Figure 17 for more details of the CB external force and whipping vibrations.

3 Catamaran model motions

The heave and pitch Response Amplitude Operators (RAOs) of the catamaran model with different centre bow and wet-deck configurations were determined using the LVDT data, Figures 12 and 13 show the motion RAOs in 90 mm waves. In these figures, the dimensionless heave (H^*) is $H^* = \frac{\bar{H}_a}{\bar{\zeta}_a}$, where, $\bar{H}_a$ is the average heave amplitude and ($\bar{\zeta}_a$) and is the average wave amplitude. The dimensionless pitch (P^*) is $P^* = \frac{\bar{\theta}_a}{\frac{2\pi\bar{\zeta}_a}{\lambda}}$, where, $\bar{\theta}_a$ is the average pitch amplitude, and $\frac{2\pi\bar{\zeta}_a}{\lambda}$ is the maximum wave slope defined as a function of average wave amplitude ($\bar{\zeta}_a$) and wavelength (λ). The dimensionless wave encounter frequency (ω_e^*) is $\omega_e^* = \omega_e \sqrt{\frac{L}{g}}$,where ω_e is the circular wave encounter frequency, L is the model overall length and g is gravitational acceleration.

As shown in Figure 12 (a), the high wet-deck catamaran has the higher dimensionless heave amplitude (H^*) compared to parent wet-deck design, whereas the difference between the low wet-deck and parent wet-deck in H^* is not significant. In contrast, the effect of wet-deck vertical position on dimensionless pitch amplitude (P^*) is small as shown in Figure 13(a). The long, parent and short CBs have on the other hand more similar dimensionless heave amplitude than dimensionless pitch amplitude, as can be seen in Figures 12 (b) and 13 (b).

Both H^* and P^* show a significant decrease from the frequency of maximum dimensionless heave and pitch to the higher wave encounter frequencies. At a model speed of 2.89 m/s, the pitch and heave peak frequencies for different CB configurations are in the range of $\omega_e^* = 3 - 4$, which corresponds

with the wavelength ratio (λ/L_m) in the range 1.7 to 2.3 as shown in the 2nd x-axis of Figures 12 and 13. In addition, both heave and pitch amplitudes approach minimal values when wavelength (λ) is slightly shorter than the overall model length (L_m).This is expected since there would be roughly equal positive and negative sectional force contributions over a wavelength.

4 Slam characterisation

The slamming process of the catamaran model in regular waves was identified using data obtained from video recordings. Two different types of slam were identified, which will be termed 'long wavelength slam' and 'short wavelength slam'. The main differences between these are the catamaran motions and centre bow immersion at the slamming instants. In long waves the centre bow tends to dive into waves with large bow motion but in short waves it tends to pierce through waves with small bow motion.

Figure 14 shows photographs of the hydroelastic catamaran model encountering a typical long wavelength slam at a speed of 2.89 m/s in 90 mm waves of dimensionless encounter frequency $\omega_e^* = 4.5$. The photographs are extracted in increments of 0.1 s (i.e. increments of six frames from a video file recorded at a rate of 60 frames per second). After the centre bow entry in waves (see Figure 14 (a1-a3)), the immersion increased to the point that the water filled the archways. During the immersion stage jets of water were directed up either side of the arch, meeting near the top at an instant in time termed 'arch closure' (Lavroff and Davis, 2015). After the arch closure, the slam took place within a few milliseconds, exerting an impulse onto the centre bow. Figure 14 (a4) indicates the post slamming process in which the merged jets were expelled forward and aft forming water spray in the centre bow area while the centre bow exits the water. The centre bow continues to rise until it reaches its highest vertical position, which is shown in Figure 14(a6).

The short wavelength slam type, however, was observed when the model motions were small and thus the centre bow had low amplitude in vertical displacement. A typical example of this slam type is shown in Figure 15, which presents photographs of the catamaran model at $\omega_e^* = 6.7$. As is evident, the arch closure and the formation of the water spray in Figure 15 are less severe compared to that seen in Figure 14, suggesting that the catamaran model experienced less severe impact loads at the higher wave encounter frequencies as will be seen later in this paper.

It is valuable to identify the effects of heave and pitch motions on slamming occurrences of the catamaran model. Since the heave and pitch motions do not provide a direct indication of wet-deck

slam occurrences at each encounter frequency, additional information regarding the heave and pitch phases and encountered wave profile is required for such evaluation. However, the measurement of the heave and pitch motion and encountered wave at the LCG does enable determination of the vertical displacement along the hull relative to water surface which can be used for evaluation of slamming occurrences at different longitudinal positions along the wet-deck. The calculation method of relative displacement along the hull through experimental measurements has been comprehensively reported in (Shabani et al., 2018).

Using relative motion analyses, the results provided by Shabani et al.(2018) indicated that the 2.5 m catamaran model was vulnerable to wet-deck slamming in 60 mm wave height or greater at a speed of 2.89 m/s for all tested CB configurations. It was found that the amplitude of relative vertical displacement of the catamaran model in regular waves increases significantly from midship to the bow and exceeds the catamaran wet-deck clearance at a certain longitudinal distance from midship depending on the wet-deck vertical position in each case.

It is worth noting that the calculations of relative vertical displacement in (Shabani et al., 2018) were conducted using an undistributed wave profile along the hull. However, as shown in Figures 14 and 15, the video recordings also indicated that the centre bow entry in waves forms significant water disturbances (lateral jet flows) prior to the slamming occurrences. Such consideration is important for the identification of slamming events using the relative motion method, especially when timing for slam identification is important.

Figure 16 shows the vertical displacement relative to the undisturbed water surface along the hull length at the instant of slamming for the catamaran model with parent CB configuration at two encounter frequencies of ω_e^* = 4.5 and 6.7 in 90 mm waves at a speed of 2.89 m/s.

The run time instants shown in Figure 16 (a & b) correspond to times at which the vertical forces acting on the centre bow segment, shown by thick vertical lines near to the centre bow truncation, were maximum during the encountered wave cycles. The vertical positions of the model along the hull were calculated from the heave and pitch at the slamming instants. The wave profiles along the model were also reconstructed by extrapolation of the undisturbed wave profiles measured by the wave sensor at the point aligned with the LCG of the model.

It can be seen in Figure 16 (a & b) that the undisturbed wave profiles at slamming instants do not contact at any point with either the flat wet-deck, which is extended from the centre bow truncation to

the catamaran model transom, or the arch top above the centre bow. Note that the tunnel clearance is approximately 67 mm and the centre bow length is 608 mm as motioned earlier in Table 3 for the parent CB. However, Figure 16 (a & b) shows that the centre bow was, to a high degree, immersed while strong slamming loads were measured at both encounter frequencies. Since the undisturbed wave profiles at slamming indicate the arch top is not in contact with water in both encounter frequencies, the wave impacts identified had to be due to the water uprise within the archways during the centre bow entry as seen in the video frames presented above. Therefore, although analysis regarding the vertical displacement relative to undisturbed water surface can indicate the vulnerability to slamming for WPCs with a centre bow, it cannot accurately indicate the instants at which arch top slamming occurs. The measurement of loads acting on the centre bow is then critical to obtain the wave profile at the slamming instant and to estimate the centre bow immersion at or prior to slamming for design analysis.

Figure 16 indicates that both centre bow immersion and slam loads are greater at $\omega_e^* = 4.5$ compared to those at $\omega_e^* = 6.7$, suggesting a connection between the volume of water displaced by the centre bow and the severity of slamming at a given speed and wave height. This connection also suggests that the arch filling or arch closure are spatially broader at $\omega_e^* = 4.5$ compared to that at $\omega_e^* = 6.7$ as the slamming is caused by arch closure during the centre bow entry.

The effects of the time-average sinkage and trim of the catamaran model in waves on slamming occurrences are also important. The mean level of time records of heave and pitch showed that the catamaran model at a speed of 2.89 m/s experiences sinkage and trim bow-up during the regular wave tests, especially at high wave encounter frequencies. The catamaran model sinkage and lateral jet flow due to the entry of the centre bow and demihulls both increase the propensity to slam, as opposed to bow up trim.

As seen in Figures 12 and 13, at a wave encounter frequency $\omega_e^* = 6.7$ the heave and pitch amplitudes of the catamaran model were small when the wavelengths were shorter than the catamaran length. In the absence of the large heave and pitch motions that occur in larger waves, the slamming at $\omega_e^* = 6.7$ was caused mainly by the model sinkage and wave elevations underneath the connecting structure between the centre bow and demihulls. In contrast, slamming at $\omega_e^* = 4.5$ was caused by more excessive heave and pitch motions while the wave elevation was not as significant. This

difference can be an important consideration for the design of an active ride control system or a novel centre bow configuration for slam alleviation.

A pitch damping RCS can thus provide an effective approach for reducing slamming loads when slamming is due to pitch-in of the centre bow (i.e. in the long wavelength slam type). However, when slamming is due to the centre bow piercing through waves (i.e. the short wavelength slam type), a modification of the arch wet-deck geometry can be the best approach to minimise slamming load.

5 Identification of slam loads

The load measurements included both centre bow entry and slamming loads excluding the demihull entry load. The slamming loads were disaggregated from the centre bow entry loads to avoid over prediction of the arch wet-deck slam loads. The disaggregation of loads was important regarding the centre bow design because the bow entry load that provides the pitch restoring moment is indeed a positive aspect of the introduction of the centre bow for seakeeping purposes. In contrast, the arch wet-deck slam load is a negative consequence of the introduction of the centre bow.

Figure 17 presents an example of the time profile of the vertical forces acting on the CB segment. The peak external load acting on the CB segment was divided into two main components. The first is the maximum force due to hydrodynamic pressure variations over the lower central surface of the centre bow which does not extend to the higher arch wet-deck surfaces. This force is referred to as the bow entry load. The second is the rapid slam force acting on the wet-deck and the cross archway structure. The peak slam force (F^{slam}), hereafter referred to as just the slam force, is

$$F^{\mathrm{slam}} = F^{\mathrm{max}} - F^{\mathrm{be}}, \qquad (2)$$

where, F^{max} is the peak force acting on the CB segment at the slam instant, and F^{be} is the maximum bow entry force estimated by applying a 5$^{\mathrm{th}}$ order low pass Butterworth filter with 5 Hz cutoff frequency on the CB force signal.

Although the results were not substantially independent of changes to the cutoff frequency owing to the transient nature of slamming forces, the choice of 5 Hz cutoff frequency appeared to give a good estimation of the bow entry force after testing different cutoff frequencies. The target was to identify

the trend of the underlying wave load without including the slamming effects by increasing the cutoff frequency from an initial value that was twice the wave encounter frequency for each run.

The CB segment experienced two types of vibrations evident in the force signals: first, the CB segment vibrations on its mountings, which appear as high-frequency oscillations (65–75 Hz) after the peak slam load; and second, the CB segment vibrations due to the forward segment whipping, which appear as 12–14 Hz oscillations (Lavroff, 2009; Rafie Shahraki, 2014). Since these vibrations occur after and in response to a slamming event and decay quickly, the contributions of these forces on the slam forces are negligible.

It is worth noting that, in terms of time scale, the duration of slam loads (~15ms) were significantly longer than the period of the specified resonance frequency of the individual bow mounting load cells in the vertical direction (4.9 kHz). However, owing to the influence of the stiffness of the transverse beams and the effective centre bow mass, the measured resonant frequency of the combined bow mounting system was found to be in the range between 65-75 Hz. Thus the duration of a typical slam event was similar to the period of the centre bow vibrating vertically on the transverse beam mountings. Therefore, whilst the response of the bow on its mountings may be regarded as approximately quasi-static, further investigation of the effect of the dynamics of the centre bow mountings is desirable.

Figures 18 and 19 show the vertical component of loads acting on the centre bow segment of HSM02 catamaran model with different centre bow and wet-deck configurations at a speed of 2.89 m/s in 60 mm and 90 mm waves. The CB segment loads are shown in the top row (a1 and b1) and below them (a2, b2, a3 and b3) are the disaggregated slam and bow entry forces respectively.

Although the model tests were conducted in regular waves, the peak CB total forces showed significant variations from the mean values within a single run. In these graphs, the markers show the mean forces and the error bars present the 95% confidence bounds of the mean. The highest peak or the lowest peak in a single run was not necessarily located at the early stage of the test, suggesting the variation was not due to start-up transients. In addition, in some cases the small strength slam loads were often followed by a strong slam load while the consecutive wave cycles were quite similar. These observations were particularly the case for $\omega_e^* > 6$ in which the slam load variability seemed to be persistent regardless of the run time. However, it was observed from the measured load time traces that the variability of peaks reduced as the time through the run increased for most of the encounter wave frequencies in which $\omega_e^* < 6$.

The results in Figure 18 (a2) show that the slam occurrences and slam severity decrease as the wet-deck height increases for 60 mm waves. The high CB appears to show slam occurrences for the range $\omega_e^* = 4.5 - 5.1$, with maximum slam loads averaging 75 N, in comparison with the low CB and parent CB with maximum slam loads averaging 115 and 90 N respectively. However, in 90 mm waves as shown in Figure 19 (a2), the maximum slam loads for the high, parent and low CBs are almost similar averaging just less than 200 N. The slam loads on the high CB tend to be lower than slam loads on the low and parent CBs for $\omega_e^* > 5.5$, and it approaches one third of the low and parent slam loads at $\omega_e^* = 6.3$.

As shown in Figures 18 (b2) and 19 (b2), the vertical slam loads increase with the increase in the centre bow length. Maximum slam loads for the long CB and short CB in 90 mm waves are approximately 270 N and 120 N in comparison with 190 N in the case of the parent CB. The maximum slam loads in 60 mm waves are 55, 90 and 160 N for the short, parent and long CB respectively. The frequencies of maximum slam loads for the short and parent CB are in the range $\omega_e^* = 4.5 - 4.6$, and are in the range $\omega_e^* = 4.8 - 5.2$ for the long CB. It can be also seen that the higher wave height results in a wider range of encounter frequencies with slam occurrences.

Further analysis of these results showed that the maximum bow entry loads for different CB configurations were between 26% and 43% of the maximum total loads acting on the centre bow, with the short CB having the highest and the long CB having the lowest ratios among all CB variants. Consequently, the slam load contribution to the maximum total segment loads at high speed was as low as 57% (short CB) but as high as 74% (long CB) considering both wave heights.

As shown in Figure 19 (b1), the long CB experienced strong vertical loads averaging 365 N, which is 1.37 times the catamaran model weight. In the same condition the parent CB experienced vertical loads averaging 276 N, which was only slightly above the model weight, and the short CB experienced maximum CB loads of 71% of the model weight, the lowest CB vertical force among the various bow configurations in 90 mm waves at a speed of 2.89 m/s. The contrast was even greater when we consider the disaggregated slam force, highlighting the dramatic influence of the centre-bow length in these conditions.

6 Vertical bending moments

As detailed in Section 2, strain gauges were attached to the four elastic links at the forward and aft cuts of the HSM02 segmented model to measure the vertical bending moments (VBMs) at the forward and aft cuts. Figure 20 shows typical time records of the forward and aft VBMs for the catamaran model with the parent CB in 90 mm waves at a speed of 2.89 m/s. The peaks and troughs show the extreme sagging and hogging moments respectively. As shown, the sagging moment is notably higher than the hogging moment. Despite the similarity between the aft and forward VBM signals in terms of transient vibrations or whipping and the extreme hogging moments (Lavroff, 2009), the peak sagging moments measured in the forward link are slightly higher than that in the aft elastic link.

Figure 21 also presents the forward VBM (unfiltered and filtered) and the CB measured load for two slam events within the run above, the purpose being to show the correlation between the slam force and the VBM response. As described earlier, the catamaran model slam events occur after the centre bow entry in waves. The sagging moment increases gradually during the centre bow entry and reaches its maximum after the peak slam load. A delay of about 0.03 s can be observed between the peaks of these two signals. Similarly to the disaggregated CB loads, slam induced sagging and hogging moment components of the total VBM were isolated by subtracting a low pass filtered version of the VBM. These components are indicated in Figure 21.

The filtered VBM is obtained by a fifth order zero-phase low pass filter with 5 Hz cut-off frequency. As shown in Figure 21, the slam induced sagging and hogging moments, as well as whipping responses are superimposed on the low frequency moment component. The low frequency bending moment is associated with the catamaran model interaction with waves and includes the effect of the contributing buoyancy variations, wave excitation forces, model weight and inertial loads. The contributing inertia loads are due to the vertical accelerations caused by the heave and pitch motions.

The effect of slamming on sagging and hogging bending moments can be significant depending on the severity of slamming (Lavroff, 2009). This can be analysed by comparing the slam induced sagging and hogging moments with the peak sagging and hogging moments of the unfiltered VBM. For example, as shown in Figure 21, the slam induced sagging and hogging moments are, respectively, about 45% and 66% of the maximum sagging and hogging moments for the slam event that occurred a few milliseconds before time t =5 s.

The whipping response, which could be used for stress and fatigue analysis, can be obtained by subtracting the low pass filtered VBM from the measured VBM (Dinsenbacher and Engle, 2011). The whipping analysis procedure may involve statistical analysis to develop prediction models to explore the maximum lifetime of the ship structure (Dinsenbacher and Engle, 2011). Figure 22 shows the effects of centre bow length and wet-deck height on the total sagging and hogging moments measured at the forward cut of the catamaran model in 60 and 90 mm waves at a speed of 2.89 m/s. Similarly, Figure 23 shows total sagging and hogging moments obtained for the aft cut. The positive values show sagging moments and negative values show the hogging moments. As shown, the sagging moment increases with the increase of the length of the centre bow and decreases with the increase of the wet-deck height. These effects are more apparent from results presented at the forward cut. The effects of the centre bow length and wet-deck height on the sagging moments were similar to that seen with regard to the effect of these geometrical parameters on the slam loads. It was seen that the slam load increased as the centre bow length increased and the slam loads decreased when the wet-deck height increased. Consequently, the slam induced bending moments follow similar trends.

The results show that the effect of the bow length on the hogging moments is small and that the parent, long and short CBs have almost similar hogging moments. The high CB also shows a slightly higher hogging moment compared to the low and parent CBs. In addition, it is apparent that the hogging moments are generally smaller than the sagging moments, especially in larger waves. This difference can be attributed to the centre bow entry and exit and transient dynamic response of the hull to the slam load that can cause asymmetric structural responses in sag and hog. Overall, the sagging moments at the aft cut were slightly smaller than the sagging moment at the forward cut for different CB configurations and different test condition. This is consistent with results obtained for the parent CB from the previous scale model investigations (Lavroff, 2009; Rafie Shahraki, 2014).

7 Conclusions

In the absence of class rules addressing the link between the centre bow slam loads and structural bending loads in the main hulls of WPCs, a series of model tests has been performed to investigate how the centre bow length and wet-deck height affect the structural loads of a 112 m wave-piercing catamaran. It was found that the slamming force increases as the centre bow length increases or as the wet-deck height decreases. Therefore, there are some benefits in both reducing the centre bow length and increasing the tunnel clearance for slam reduction.

At a speed of 2.89 m/s and in 90 mm waves (full scale-equivalent to 38 knots and 4 m significant wave height) the model with the long CB experienced the largest vertical slam loads averaging 270 N, which was approximately equivalent to the catamaran model displacement. The largest slamming loads at a similar test condition for the parent CB and short CB were averaging approximately 70% and 45% of the model displacement respectively. The maximum vertical bow entry forces at the above test condition were 37%, 31% and 26% of the model displacement for the long, parent and short CBs respectively. Since the total force acting on the CB segment was equivalent to the summation of the slamming force and maximum bow entry force, the total vertical forces were 137%, 101% and 71% of the model displacement for the long, parent and short CBs respectively.

The maximum slam loads and centre bow entry loads for the high CB and low CB were almost in the same range as that obtained for the parent CB in 90 mm waves at 2.89 m/s. However, in waves with high encounter wave frequency $\omega_e^* > 6$, the high CB showed a significant reduction in slamming load compared to the parent and low CBs. The effects of high CB and low CB on slamming loads were smaller than the effects of the long CB and short CB on slamming loads.

The effects of the centre bow length and wet-deck height on the maximum sagging moments were similar to those seen with regard to the effect of these geometrical parameters on the slam loads. Thus, attention should be paid to determining the global design loads in WPCs as a function of the centre bow geometry as class rules currently neglect such a major influence.

It was seen that the short CB was the best design for the alleviation of slam loading and the long CB was the worst configuration. The high CB was the second best choice for operation in moderate waves. These findings suggest that a short centre bow plus a high wet-deck design would be highly beneficial from a structural perspective and can be further investigated in future research. Such a configuration would be particularly optimal for operation in short waves for which the heave and pitch amplitudes are small regardless of the centre bow configuration. However, the results showed that the high CB was the worst configurations in terms of heave and pitch motions among various CB configurations tested. Such a nominated configuration would be unfavourable for motions in long waves in which the amplitudes of motion are significant; it is also noted that the short CB may not be preferred when the motions are large because of the lack of reserve buoyancy. The current study suggests that conclusions for optimal design may vary as they depend very much on the design objectives, and further investigations on centre bow kinematics at slamming are recommended.

8 Acknowledgements

This work was undertaken in collaboration between the University of Tasmania, Revolution Design and International Catamarans Tasmania (INCAT) through the support of the Australian Research Council Linkage Grant number LP0883540. The work of Dr Jalal Rafie Shahraki in the development and production of the hydroelastic segmented model is also gratefully acknowledged.

9 References

AlaviMehr, J., 2016. The Influence of Ride Control Systems on the Motion and Load Response of a Hydroelastic Segmented Catamaran Model. PhD Thesis, University of Tasmania.

AlaviMehr, J., Lavroff, J., Davis, M.R., Holloway, D.S., Thomas, G.A., 2017a. An Experimental Investigation of Ride Control Algorithms for High-Speed Catamarans Part 1: Reduction of ship motions. Journal of Ship Research 61 (1), 35-49.

AlaviMehr, J., Lavroff, J., Davis, M.R., Holloway, D.S., Thomas, G.A., 2017b. An experimental investigation of ride control algorithms for high-speed catamarans Part 2: Mitigation of wave impact loads. Journal of Ship Research 61 (2), 51-63.

Amin, W., 2009. Non-linear unsteady wave loads on large high-speed wave piercing catamarans. PhD Thesis, University of Tasmania.

Shabani, B., Lavroff, J., Holloway, D.S, Davis ,M.R., Thomas, G.A, 2018. The influence of the centre bow and wet-deck geometry on motions of wave piercing catamarans. Proceedings of the Institution of Mechanical Engineers Part M: Journal of Engineering for the Maritime Environment, 1475090217753761.

Davis, M.R., Amin, W.A.I., Lavroff, J., Holloway, D.S., Thomas, G.A., Matsubara, S., Roberts, T., 2009. Global and Slam Load Model Testing to Support Developing HSMV Operations in Severe Sea Conditions, in: Rina (Ed.), International Conference for Innovation in High Speed Marine Vessels. RINA, Fremantle, Australia, pp. 93-102.

Davis, M.R., French, B.J., Thomas, G.A., 2017. Wave slam on wave piercing catamarans in random head seas. Ocean Engineering 135, 84-97.

Davis, M.R., Lavroff, J., French, B., Thomas, G.A., Holloway, D.S., Roberts, T.R., 2010. The prediction of wetdeck slam loads on high-speed catamarans, in: Adrian, B. (Ed.), International Maritime Conference, Pacific. Maritime Australia Limited, Sydney, Australia, p. CD Rom.

Dessi, D., 2013. Reconstruction of the experimental slamming force distribution based on POD, ASME 2013 32nd International Conference on Ocean, Offshore and Arctic Engineering. American Society of Mechanical Engineers, Nantes, France, pp. V009T012A057-012 pages.

Dessi, D., Ciappi, E., 2013. Slamming clustering on fast ships: From impact dynamics to global response analysis. Ocean Engineering 62, 110-122.

Dessi, D., Mariani, R., 2008. Analysis and prediction of slamming-induced loads of a high-speed monohull in regular waves. Journal of Ship Research 52 (1), 71-86.

Dinsenbacher, A., Engle, A., 2011. Guidelines for Hydroelastic Model Design, Testing and Analysis of Loads & Responses. Tech. rept. NSWCCD-TR-65-2010/12. Naval Surface Warfare Center Carderock Division.

Faltinsen, O., Chezhian, M., 2005. A generalized Wagner method for three-dimensional slamming. Journal of Ship Research 49 (4), 279-287.

Faltinsen, O.M., 2005. Hydrodynamics of high-speed marine vehicles. Cambridge University Press.

French, B.J, Thomas, G.A., Davis, M.R., 2014. Slam characteristics of a high-speed wave piercing catamaran in irregular waves. Royal Institution of Naval Architects. Transactions. Part A. International Journal of Maritime Engineering 156 (Part A1), A25-A36.

French, B.J., 2012. Slamming of large high-speed catamarans in irregular seas. PhD Thesis, University of Tasmania.

French, B.J., Thomas, G.A., Davis, M.R., 2013. Slam occurrences and loads of a high-speed wave piercer catamaran in irregular seas. Institution of Mechanical Engineers. Proceedings. Part M: Journal of Engineering for the Maritime Environment (Online FIrst), 1-13.

Ge, C., Faltinsen, O.M., Moan, T., 2002. Global hydroelastic response of a catamaran due to wetdeck slamming accounting for forward speed, ASME 2002 21st International Conference on Offshore Mechanics and Arctic Engineering. American Society of Mechanical Engineers, Oslo, Norway, pp. 221-230.

Kapsenberg, G.K., 2011. Slamming of ships: where are we now? Philosophical Transactions of the Royal Society of London A: Mathematical, Physical and Engineering Sciences 369 (1947), 2892-2919.

Lavroff, J., 2009. The Slamming and Whipping Vibratory Response of a Hydroelastic Segmented Catamaran Model. PhD Thesis, University of Tasmania.

Lavroff, J., Davis, M., Holloway, D., Thomas, G., 2013a. Wave slamming loads on wave-piercer catamarans operating at high-speed determined by hydro-elastic segmented model experiments. Marine Structures 33, 120-142.

Lavroff, J., Davis, M.R., 2015. Slamming kinematics, impulse and energy transfer for wave-piercing catamarans. Journal of Ship Research 59 (3), 145-161.

Lavroff, J., Davis, M.R., Holloway, D.S., Thomas, G., 2011. Determination of wave slamming loads on high-speed catamarans by hydroelastic segmented model experiments. International Journal of Maritime Engineering 153 (A3), 185-197.

Lavroff, J., Davis, M.R., Holloway, D.S., Thomas, G., 2013b. Wave slamming loads on wave-piercer catamarans operating at high-speed determined by hydro-elastic segmented model experiments. Marine Structures 33, 120-142.

Lavroff, J., Davis, M.R., Holloway, D.S., Thomas, G.A., 2009. The Vibratory Response of High-Speed Catamarans to Slamming Investigated by Hydroelastic Segmented Model Experiments. International Journal of Maritime Engineering 151 (4), 1-13.

Matsubara, S., 2009. Ship Motions and Wave-Induced Loads on High Speed Catamarans. PhD Thesis, University of Tasmania.

McVicar, J., Lavroff, J., Davis, M.R., Davidson, G., 2014. Transient slam load estimation by RANSE simulation and by dynamic modeling of a hydroelastic segmented model, The 30th Symposium on Naval Hydrodynamics, Hobart, Tasmania, pp. 1-16.

McVicar, J., Lavroff, J., Davis, M.R., Thomas, G.A., 2016. Slam excitation scales for a large wave piercing catamaran and the effect on structural response, 13th International Conference on Fast Sea Transportation. SNAME, Washington DC, USA, pp. 1-10.

Ochi, M.K., 1964. Prediction of occurrence and severity of ship slamming at sea, Fifth symposium of naval hydrodynamics. Office of Naval Research, Bergen, Norway, pp. 545-596.

Ochi, M.K., Motter, L.E., 1973. Prediction of slamming characteristics and hull responses for ship design. Trans. SNAME 81, 144–176.

Rafie Shahraki, J., 2014. The influence of hull form on the slamming behaviour of large high speed catamarans. PhD Thesis, University of Tasmania.

Thomas, G., 2003. The Slamming of Large High Speed Catamarans. PhD Thesis, University of Tasmania.

Thomas, G., Davis, M., Holloway, D., Roberts, T., 2003a. The whipping vibration of large high speed catamarans. International Journal of Maritime Engineering 145, 289-304.

Thomas, G., Davis, M., Holloway, D., Watson, N., Roberts, T., 2003b. Slamming response of a large high-speed wave-piercer catamaran. Marine Technology 40 (2), 126-140.

Thomas, G., Winkler, S., Davis, M., Holloway, D., Matsubara, S., Lavroff, J., French, B., 2011. Slam events of high-speed catamarans in irregular waves. Journal of Marine Science and Technology 16 (1), 8-21.

Thomas, G.A., Davis, M.R., Holloway, D.S., 2003c. The whipping vibration of large high speed catamarans. International Journal of Maritime Technology 145, 289-304.

Thomas, G.A., Davis, M.R., Holloway, D.S., Roberts, T., 2002. Extreme Asymmetric Slam Loads on Large High Speed Catamarans, in: Pensa, C. (Ed.), 6th Symposium on High Speed Marine Vehicles. University of Naples, Castello di Baia, Italy, pp. I.15-I.23.

Thomas, G.A., Davis, M.R., Holloway, D.S., Roberts, T., 2004. An Investigation into the Whipping of Large High-Speed Catamarans, in: Volker, B. (Ed.), HIPER 04: 4th International Conference on High-Performance Marine Vehicles. INSEA, Rome, Italy, pp. 162-176.

Thomas, G.A., Davis, M.R., Holloway, D.S., Roberts, T., 2005. The influence of slamming and whipping on the fatigue life of a high-speed catamaran, in: Prof Kirill, V.R. (Ed.), FAST: International Conference on Fast Sea Transportation. Institute of Marine Engineering, Science and Technology, St Petersburg, Russia, pp. 1-8.

Thomas, G.A., Davis, M.R., Holloway, D.S., Roberts, T., 2008. The Vibratory Damping of Large High Speed Catamarans. Marine Structures 21 (1), 1-21.

Thomas, G.A., Davis, M.R., Holloway, D.S., Roberts, T.R., 2006. The effect of slamming and whipping on the fatigue life of a high speed catamaran. Australian Journal of Mechanical Engineering 3 (2), 165-174.

Von Karman, T., 1929. The impact on seaplane floats during landing, Technical Note 321. NACA, Washington.

Wagner, H., 1932. Phenomena associated with impact and gliding on a liquid surface. Journal of Applied Mathematics and Mechanics 12 (4), 193-215.

Zhao, R., Faltinsen, O., 1993. Water entry of two-dimensional bodies. Journal of Fluid Mechanics 246, 593-612.

Figure Captions

Figure 1(a) A wave piercer catamaran with an above water centre bow (http://www.incat.com.au/).

(b) The buckling of the hull structure near the bridge as a consequence of severe slamming loads for a 96-m WPC (Lavroff et al.(2013))

Figure 2 (a) The 2.5 m segmented catamaran model (HSM02) of the 112-m Incat wave-piercing catamaran, showing the forward middle and aft segments (b) Exploded views of the demihulls, flat wet-deck and centre bow segment of the catamaran model HSM02.

Figure 3 Schematic plan view of the HSM02 model showing the configuration of backbone beams and the locations of elastic links.

Figure 4 The catamaran model HSM02 with the parent CB.

Figure 5 Profile view of the catamaran model, illustrating the tunnel clearance and centre bow length.

Figure 6 (a) Photographs of the parent and long CBs extenders (b) Photograph of the HSM02 catamaran model with the short CB.

Figure 7 The HSM02 catamaran model with (a) the low CB (b) the high CB at initial stage of towing in calm water

Figure 8 Locations of sensors used for the 2.5 m hydroelastic segmented catamaran model. Refer to Table 4 for symbols corresponding to different sensors.

Figure 9 Representation of vertical loads acting on the centre bow segment.

Figure 10 Comparison of the CB segment accelerations between the measured data and filtered data during wave slamming on the centre bow at $\omega_e^* = 4.5$ for a speed of 2.89 m/s in 90 mm wave height. The dimensionless wave encounter frequency (ω_e^*) is $\omega_e^* = \omega_e \sqrt{\frac{L}{g}}$,where ω_e is the circular wave encounter frequency, L is the model overall length and g is gravitational acceleration.

Figure 11 CB vertical load sensed by load cells (top), CB vertical inertia load (middle) and CB vertical force (bottom) for the parent CB at $\omega_e^* = 4.5$ for a speed of 2.89 m/s in 90 mm wave height.

Figure 12 Dimensionless heave responses of the catamaran model with different centre bow and wet-deck configurations at a speed of 2.89 m/s in 90 mm wave heights. The dimensionless heave (H^*) is $H^* = \frac{\bar{H}_a}{\bar{\zeta}_a}$, where, $\bar{H}_a$ is the average heave amplitude and ($\bar{\zeta}_a$) and is the average wave amplitude.

Figure 13 Dimensionless pitch responses of the catamaran model with different bow length and wet-deck configurations at a speed of 2.89 m/s in 90 mm wave height. The dimensionless pitch (P^*) is $P^* = \frac{\bar{\theta}_a}{\frac{2\pi\bar{\zeta}_a}{\lambda}}$, where, $\bar{\theta}_a$ is the average pitch amplitude, and $\frac{2\pi\bar{\zeta}_a}{\lambda}$ is the maximum wave slope defined as a function of average wave amplitude ($\bar{\zeta}_a$) and wavelength (λ).

Figure 14 HSM02 catamaran model with the parent centre bow configurations experiencing a slam event at $\omega_e^* = 4.5$ for a speed of 2.89 m/s in 90 mm wave height.

Figure 15 HSM02 catamaran model with the parent centre bow configurations experiencing a slam event at $\omega_e^* = 6.7$ for a speed of 2.89 m/s in 90 mm wave height.

Figure 16 The catamaran slamming instants at (a) $\omega_e^* = 4.5$ and (b) $\omega_e^* = 6.7$, representing two different slam situations due to (a) combined heave and pitch motion in waves and (b) combined model sinkage and wave elevation within archways.

Figure 17 The vertical bow entry and slam forces acting on the parent CB for a slam event at $\omega_e^* = 4.5$ at a speed of 2.89 m/s in 90 mm wave height.

Figure 18 Vertical forces acting on the centre bow segment of HSM02 catamaran model with different centre bows and wet-deck configurations at a speed of 2.89 m/s in 60 mm waves.

Figure 19 Vertical forces acting on the centre bow segment of HSM02 catamaran model with different centre bows and wet-deck configurations at a speed of 2.89 m/s in 90 mm waves.

Figure 20 Time records of the forward and aft (starboard) vertical bending moments for the parent CB in 90 mm waves at a model speed of 2.89 m/s.

Figure 21 Vertical bending moment measured at the forward elastic link (starboard) and load measured on the centre segment for the parent CB in 90 mm waves at a model speed of 2.89 m/s.

Figure 22 Forward cut total sagging *(positive) and hogging **(negative) moments for various centre bow and wet-deck configurations at different test conditions.

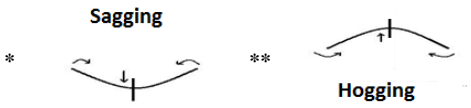

Figure 23 Aft cut total sagging* (positive) and hogging **(negative) moments for various centre bow and wet-deck configurations at different test conditions.

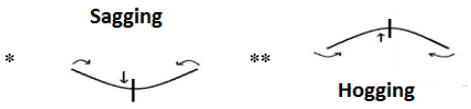

Abbreviation List

Australian Maritime College (AMC)
Centre bow (CB)
Computational Fluid Dynamics (CFD)
Det Norske Veritas (DNV)
Hydroelastic segmented model (HSM)
Linear Variable Differential Transducers (LVDTs)
Longituidnal centre of gravity (LCG)
Ride control system (RCS)
Response Amplitude Operators (RAOs)
Reynolds-Averaged Navier-Stokes (RANS)
Wave-piercing catamarans (WPCs)

Nomenclature

a_z	Vertical acceleration of the centre bow segment
a_z^{fwd}	Vertical acceleration measured by the aft accelerometer
a_z^{aft}	Vertical acceleration measured by the forward accelerometer
g	Gravitational acceleration
h_w	Nominal wave height
m_{cb}	Mass of the centre bow segment
$m_{external}$	Mass of external load for calibration
t	Time
F^{be}	Maximum bow entry force
F^{max}	Maximum force acting on the centre bow segment
F^{slam}	Peak slam force acting on the centre bow segment
F_z^{slam}	Peak vertical slam force
F_z^{aft}	Vertical load measured by the aft load cell
F_z^{fwd}	Vertical load measured by the forward load cell
F_z	Total measured load in vertical direction
H^*	Dimensionless heave
$\bar{H}_{\mathrm{a}}$	Average heave amplitude
L	Overall model length
L_{cb}	Centre bow length
P^*	Dimensionless pitch
T_C	Tunnel clearance
T_H	Tunnel height
V_m	Model speed
λ	Wavelength
$\bar{\theta}_{\mathrm{a}}$	Average pitch amplitude
$\bar{\zeta}_{\mathrm{a}}$	Average wave amplitude
ω_{e}	Circular wave encounter frequency
ω_e^*	Dimensionless wave encounter frequency